Chinese Chemical Letters 34 (2023) 108015

Contents lists available at ScienceDirect

Chinese Chemical Letters

journal homepage: www.elsevier.com/locate/cclet

Atom-economic macrocyclic amphiphile based on guanidinium-functionalized selenacrown ether acting as redox-responsive nanozyme

Bo Li, Qiangqiang Xu, Xin Shen, Tiezheng Pan, Jie Shang, Yan Ge*, Zhenhui Qi*

Sino-German Joint Research Lab for Space Biomaterials and Translational Technology, Synergetic Innovation Center of Biological Optoelectronics and Healthcare Engineering (BOHE), Shaanxi Provincial Synergistic Innovation Center for Flexible Electronics & Health Sciences (FEHS), School of Life Sciences, Northwestern Polytechnical University, Xi'an 710072, China

ARTICLE INFO

Article history:
Received 31 August 2022
Revised 17 November 2022
Accepted 20 November 2022
Available online 29 November 2022

Keywords:
Selenium
Guanidinium
Macrocycle amphiphile
Crown ether
Molecular assembly
Winkled surface
Nanozyme

ABSTRACT

Control of self-assembly is significant to the preparation of supramolecular materials, but the control of hydration, responsiveness, dimension, catalysis of macrocyclic amphiphiles in an atom-economic manner is still a great challenge. The herein presented 527 Da low-molecular-weight macrocyclic amphiphile was fabricated by utilizing the selenium-containing crown ether as a hydrophobic motif together with guanidinium group as the hydrophilic moiety. The resulting benzo[21]crown-7 based macrocyclic amphiphile readily forms a redox-responsive solid nanoparticles in water, which can further interconnect into wrinkled pattern on-surface, as well as exhibits as a nanozyme for catalyzing disulfid bond formation. The present work highlights the great potential of guanidinium- and selenium-containing crown ethers for the control of functional assemblies.

Control of self-assembly is significant in preparing supramolecular materials and illustrating the diversity in natural or artificial systems [1–3]. Macrocyclic amphiphiles, which combine the features of macrocyclic compounds and classic amphiphiles, have gained considerable attention in various fields [4,5]. A wide variety of novel nanostructures self-assembled using macrocyclic amphiphiles have potential application in drug/gene delivery, cell imaging, and catalysis [6–15]. Owing to the fine-developed macrocycle chemistry, hydrophilic, hydrophobic chains, and/or functional groups can be decorated on the respective sides of the macrocyclic frameworks or through host-guest chemistry. However, despite prior research demonstrating the advantages of using macrocycles to construct novel amphiphiles, atom-economic control in hydration, responsiveness, dimension, and catalysis of the supramolecular nanostructures of macrocyclic amphiphiles remains a significant challenge [16].

Crown ethers, the first class of synthetic macrocycles, have been widely used as building blocks in the development of functional self-assemblies including molecular machines, supramolecular polymers, and sensors, albeit in the organic phase [17–26]. Recently, we and others found that crown ethers are an intriguing host for studying water-mediated non-covalent interactions [27–29]. In particular, benzo[21]crown-7 (C7) represents a new class of water-soluble crown macrocycles with high water solubility (4.21 mol/L, Table S1 in Supporting information). This value is higher than that of well-known water-soluble macrocycles (such as cucurbitu[*n*]rils and cyclodextrins) [30]. Insight into water−C7 interactions further led to the discovery of "structural water" for supramolecular adhesive materials [27,31,32], reversing the Hofmeister effect [33] and thus benefiting the communities of chemistry, materials and physics. Intriguingly, substituting one selenium (Se) atom in C7CN significantly enriches the hydration behavior of crown ether (Scheme 1a). On the one hand, the selenide group is a poor HB acceptor [34], the single Se atom exists in C7CN thus readily makes the original hydrophilic crown macrocycle becomes extremely hydrophobic (Table S1 in Supporting information). On the other hand, selenoxide, in contrast, is an excellent HB acceptor [35]; hence, the crown ether comprising it has a higher water solubility [note: the H-bond distance of the selenoxide group (1.78 Å) is shorter than that of an ether (-O-) group (1.90 Å)] [36]. Importantly, the transition between selenide and selenoixde is redox adaptive. Therefore, the site mutation of an oxygen atom in the crown ether to selenium endows redox-adaptive amphiphilicity to the crown macrocycle, which is unprecedented in previously reported macrocycles. Detailed water-

* Corresponding authors.
E-mail addresses: ge@nwpu.edu.cn (Y. Ge), qi@nwpu.edu.cn (Z. Qi).

https://doi.org/10.1016/j.cclet.2022.108015
1001-8417/

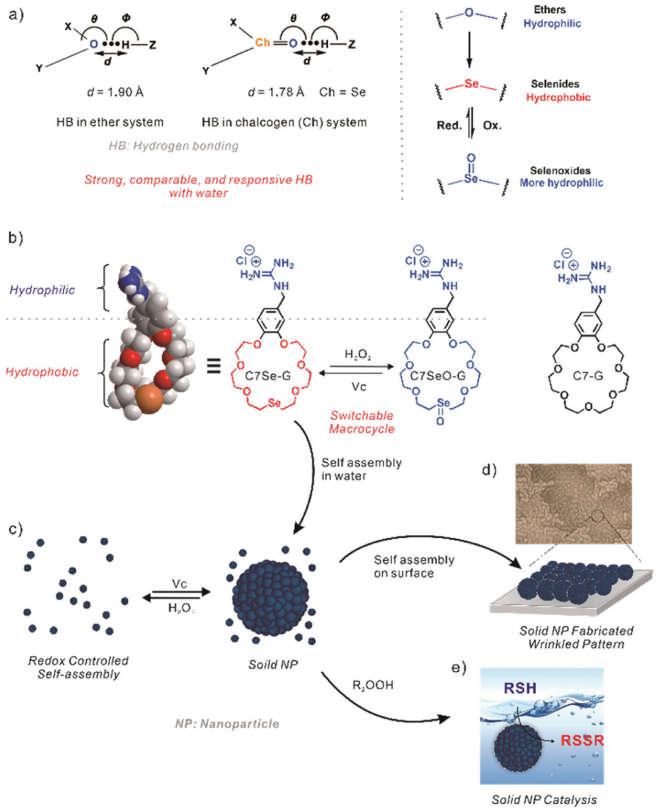

Scheme 1. (a) Design principle of adaptive and comparable hydrogen bonding behavior of selenide, selenoxide. (b) Chemical structure of guanidinium- and selenium-functionalized crown ether-based macrocyclic amphiphile C7Se-G, and its redox-switchable behavior. (c) Cartoon representation of the redox controlled self-assembly for the formation of solid nanoparticles. (d) Consequent formation of wrinkled surface *via* the self-assembly of macrocyclic amphiphile. (e) Its catalysis in aqueous medium for the formation of disulfide bonds.

solubility of diverse selenium-functionalized crown ether derivatives in Table S1. Moreover, selenium catalysis is an important area in organic synthesis, and various organic selenoxide/selenide catalysts have been reported [37–40]. Therefore, selenium-containing crown ether has fine control over hydration, redox-responsiveness, and catalysis, which is ideal for designing novel macrocyclic amphiphiles. However, thus far, in comparison to calixarenes [6,13], cucubiturils [2,14], cyclodextrins [10–12], and pillarenes [6,12–14], crown ether-based macrocyclic amphiphiles have rarely been explored [4,5,41]. Furthermore, investigation of selenium-containing crown ethers has been largely belittled in organic and solid phases [42–46], their aqueous behavior remains elusive.

On the basis of above considerations, we designed and synthesized a guanidinium- and selenium-functionalized crown ether, C7Se-G, which represents a type of "atom-economic" macrocyclic amphiphile (Scheme 1b). Guanidinium has a unique molecular structure. The guanidine moiety is incorporated in many natural products and synthetic systems of biological importance [47]. Therefore, the development of guanidinium-containing motifs is of significant interest in the fabrication of novel stimuli-responsive materials and for understanding biological processes [48]. Herein, selenium-containing crown ether served as the hydrophobic segment. With guanidinium group acting as the necessary hydrophilic moiety, the crown-ether-based macrocyclic amphiphile readily forms solid nanoparticles in water, exhibiting a redox-responsive self-assembly (Scheme 1c). Furthermore, the self-assembly of the C7Se-G solid nanoparticles can generate wrinkled surfaces (Scheme 1d). The positively charged guanidinium groups serving on the C7Se-G solid nanoparticles increased binding with the carboxylic acid group-containing substrate, which enhanced the catalytic ability of the resulting nanozyme to promote disulfide bond formation (Scheme 1e). Notably, features including redox responsiveness, wrinkled surface and nanozyme were achieved in a low-molecular-weight macrocyclic amphiphile with a molecular weight of less than 530 Da.

The design of the macrocyclic amphiphile C7Se-G is based on the guanidinium group and the selenium-containing crown ether moiety with approximately 6000 times difference in solubility, which provides the essential molecular origin of hydrophilicity and hydrophobicity for designing novel crown-ether-based amphiphile; the water solubility of guanidinium chloride reaches 573 g/L (5.99 mol/L, data from Biospectra Inc.), whereas that of selenium-containing cyanobenzo-21-crown-7 ether C7SeCN (Table S1) was only 0.44 g/L (1 mmol/L) at room temperature [34,43]. The guanylating agent, 1*H*-pyrazolecarboxamidine hydrochloride, is a common method for generating guanidinium-functionalized macrocycles, and the amino-equipped macrocycle serves as the essential precursor. Herein, we initially attempted to reduce the C7CN benzylamine[21]crown-7 ether using the BH_3-THF protocol developed by our group (Scheme 2b) [26], which has consequently been widely used by many groups [27–31,33,49]. However, it failed in this study. Instead, the Gabriel amine synthetic route works for generating amine-functionalized selenium-containing crown ether derivatives (Scheme 2a, see Supporting information for detailed description). As shown in Scheme 2a, C7Se-G was obtained in a moderate yield. C7-G was synthesized as a control with the only difference being that Se was substituted by O (Scheme 2b and Scheme S2 in Supporting information). C7-G was expected to be highly water-soluble based on the high solubility of benzo[21]crown-7 ether in water (1500 g/L, 4.21 mol/L) [30]. All compounds were characterized *via* nuclear magnetic resonance (NMR) spectroscopy, including ^{1}H, ^{13}C, and ^{77}Se NMR, and high-resolution electrospray ionization mass spectrometry (HR-ESI-MS) (Figs. S1–S16 in Supporting information).

By adding water to C7Se-G and gently shaking it, a clear aqueous solution of C7Se-G with 2 mol/L concentration can be readily obtained (Fig. S17 in Supporting information). A prominent Tyndall effect was observed (Fig. 1 and Fig. S18 in Supporting information). According to previous studies, the reversible redox reaction between selenide and selenoxide can be easily realized by introducing H_2O_2 and vitamin C (Vc). Therefore, we performed ^{1}H and ^{77}Se NMR, and ESI-MS experiments to determine the redox reactions at the molecular level. The ^{1}H NMR spectrum showed that the peaks of protons adjacent to the Se atom (marked with asterisks) at 2.79 ppm downshifted and split into two sets of peaks at 3.2 and 3.45 ppm, exhibiting a characteristic splitting pattern for the oxidization product of chalcogen-containing organic species [50]. The ^{77}Se NMR spectrum also showed a peak shift from 119.81 to 847.65 ppm (Fig. 1c). The ESI-MS data indicate that oxidation occurred, and the molecular ion peaks for C7Se-G at *m/z* 492.16 ($[M+H]^+$) disappeared after oxidation, whereas the peaks for C7SeO-G at *m/z* 508.16 ($[M+O+H]^+$) became more evident (Fig. S25 in Supporting information). The selenide peak reappeared when Vc was introduced (Fig. 1a), providing evidence of a reversible transition between C7Se-G and C7SeO-G. Furthermore, the macroscopic Tyndall effect of the C7Se-G aqueous solution disappeared and was observed again during the redox process of C7Se-G, as shown in Fig. 1b, which corresponds to the disassembly and reassembly of C7Se-G in aqueous solution. These results not only demonstrated that the solvation of C7Se-G assemblies can be readily modified in a redox-controlled manner but also presented two stable forms for organic selenide forms, which can transform each other in water.

Nanoparticles can be imaged *in situ* using cryo transmission electron microscopy (cryo-TEM) because they are organized in the

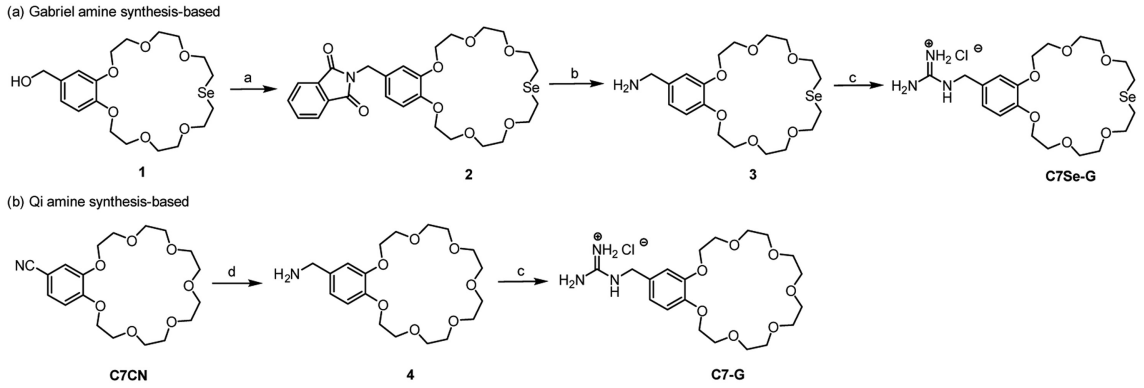

Scheme 2. The synthetic route of C7Se-G and its control C7-G. (a) Phathalimide, DIAD, $P(Ph)_3$; (b) Hydrazine hydrate (85%); (c) 1*H*-pyrazole-1-carboxamidine hydrochloride, $(i\text{-Pr})_2NEt$; (d) BH_3-THF.

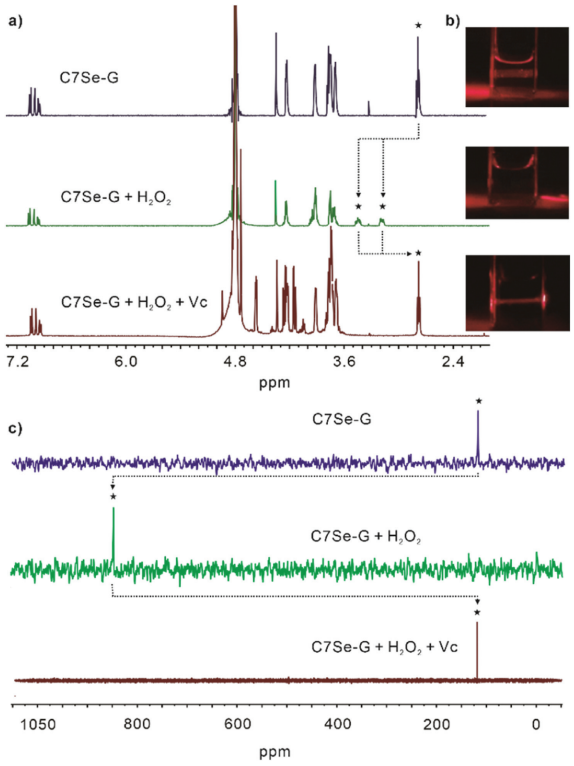

Fig. 1. Redox switches of selenide and selenoxide of C7Se-G. Star symbol show the configuration of hydrogens neighboring the selenium atom. (a) Partial ^1H NMR spectra for C7Se-G (10 mmol/L, D_2O, 500 MHz, 298 K) before oxidation, after oxidation by H_2O_2 (3 equiv.), and after further reduction with Vc (6 equiv.). (b) The inserted Tyndall images showed the macroscopic scattering effect of the responding samples in (a). (c) ^{77}Se NMR spectra for C7Se-G before oxidation (200 mmol/L, D_2O, 95 MHz, 298 K), C7Se-G after oxidation by H_2O_2 (3 equiv.) (200 mmol/L, D_2O, 95 MHz, 298 K), and C7Se-G after further reduction with Vc (6 equiv.) (180 mmol/L, D_2O, 76 MHz, 298 K).

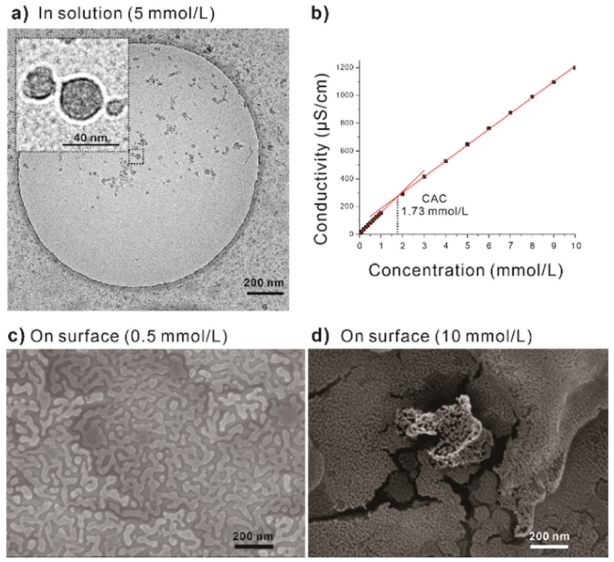

Fig. 2. (a) Cryo-TEM images of C7Se-G aggregation at the concentration of 5 mmol/L. (b) The intersection of two slopes (red lines) indicates the critical aggregation concentration (CAC) of C7Se-G was determined to be 1.73 mmol/L. SEM images of the C7Se-G aggregation at different concentration. (c) 0.5 mmol/L; (d) 10 mmol/L.

solution. Homogenous solid C7Se-G nanoparticles were visualized in the projection images of cryo-TEM in the range of 2–5 mmol/L (Fig. 2a and Fig. S19 in Supporting information). The solid nanoparticles had an average diameter of approximately 25 ± 10 nm (Fig. 2a, insert). The critical aggregation concentration (CAC) of C7Se-G was determined as 1.73 mmol/L. Diluting the aqueous solution of C7Se-G from 2 mol/L to various concentrations did not result in any significant changes upon aggregation (Fig. S18). The zeta potential results showed that the potential of 2 mmol/L C7Se-G was +7.16 mV and that its aggregates were positively charged (Fig. S22 in Supporting information).

Nanoparticle interactions are critical in a range of phenomena including protein aggregation and crystallization, reentrant phase transitions, nanoemulsion assembly and nanoparticle organization into nanowires [51]. We observed that when these positively charged solid nanoparticles are concentrated, they can form reversible self-assembled structures on surfaces that become more connected topologically (Scheme 1d and Fig. 2). Wrinkled patterns comprising C7Se-G nanoparticles with a periodic fluctuation on the surface were observed using scanning electron microscope, as shown in Figs. 2c and d. In addition, we observed that the solid nanoparticles self-assembled into larger structures have already happened at even lower concentrations of C7Se-G (*e.g.*, $c = 0.1$ mmol/L) (Fig. S20 in Supporting information). We speculate that the hydrophobic forces between the selenium-containing crown ether parts were too strong [52]. This wrinkled surface might have been caused by the interaction of Se···Se bonds. Indeed, the crystal structure of C7SeCN provides us evidence for the existence of strong intermolecular Se···Se interactions in the solid-state of selenium-containing crown ethers. From the crystal structure of C7SeCN (Fig. 3), the distance of Se···Se was determined to be approximately 3.747 Å, which is shorter than the van der Waals dis-

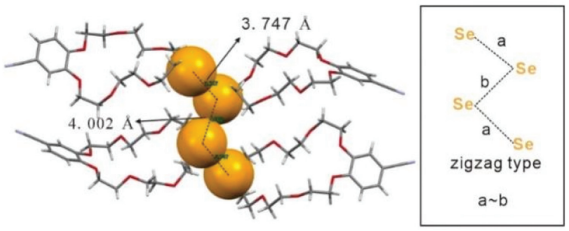

Fig. 3. Crystal structure of selenium-containing crown ether C7SeCN, which exhibits strong intermolecular Se···Se interaction.

tance between two selenium atoms (Se···Se = 4.0 Å) [53]. Moreover, the neighboring selenium-containing crown ethers fit in a typical zigzag arrangement which is in accordance with previous studies on the existence of tight chalcogen-chalcogen interactions [52]. In line with our hypothesis, after the oxidation of C7Se-G to form hydrophilic C7SeO-G, the wrinkled surface generated from the self-assembly of C7Se-G disappeared (Fig. S26 in Supporting information). The morphological transformation demonstrated that subtle changes in one atom of crown ethers can cause significant changes in their hierarchical composition and mesoscopic ordering.

The selenium(II)/(IV) redox cycle is crucial in sulfide/disulfide redox chemistry, and selenides have been studied as glutathione peroxidase (GPx) mimetics, catalyzing the reduction of peroxides using various thiols, and the formation of disulfide bonds [54–56]. Nanozymes are nanoparticles with enzyme-mimicking properties [57]. Owing to their intrinsic catalytic properties, nanozymes can modulate a series of important biological processes [58–60]. Therefore, unlike previously reported organic selenide compounds [61], the current system has the advantage of a complete reaction in water; thus, the solid nanoparticles of C7Se-G in water can readily extend the catalysis of organic selenide to aqueous substrates as nanozymes in thiol/disulfide conversion. Hydrogen peroxide (H_2O_2) and cumene hydroperoxide (CUOOH) are used as peroxide substitutes. 5-Mercapto-2-nitrobenzoic acid (MNBA) was selected as a water-soluble thiol cofactor. The decrease in ultraviolet absorbance in the oxidation of MNBA was considered a criterion for evaluating the catalytic activity for the formation of disulfide bonds. The tests were carried out in Dulbecco's phosphate-buffered saline (DPBS) at 25 °C. The turnover number (TON) provides a convenient means for comparing effectiveness. The TON of C7Se-G in the MNBA-H_2O_2 assay was 1500×10^{-4} min^{-1} (Table S2 in Supporting information). In the MNBA-H_2O_2 assay the TON of diphenyl diselenide (PhSeSePh), a typical GPx mimic, was 1.2×10^{-4} min^{-1}, indicating that C7Se-G exhibits a 1250-fold higher activity than that of PhSeSePh [62]. When H_2O_2 was replaced with CUOOH (Table S3 in Supporting information), the TON of C7Se-G was 1420×10^{-4} min^{-1}. To evaluate the catalytic effect of the guanidinium group in C7Se-G, 4-nitrobenzenthiol (NBT) was used as a comparable water-soluble thiol cofactor with a structure similar to that of MNBA but without the carboxylic acid group (Fig. 4a, box). In the NBT-H_2O_2 and NBT-CUOOH assays, the TONs of C7Se-G decreased to 120×10^{-4} and 320×10^{-4} min^{-1}, respectively. The catalytic activity of the C7Se-G assemblies in the MNBA system was significantly higher than that in the NBT system, which can be attributed to the recognition of the carboxylic acid functional group in MNBA and the guanidinium group in C7Se-G. This trend was further confirmed at 50 μmol/L concentration of C7Se-G (Fig. 4b). In contrast to C7Se-G, C7-G (Fig. S27 in Supporting information) exhibited no catalytic effect on thiol/disulfide bond conversion, indicating that the catalytic effect was due to the selenide group in C7Se-G.

In the aforementioned catalytic cycle, the Se-S linkage intermediate was generated after the reaction between thiol and selenide,

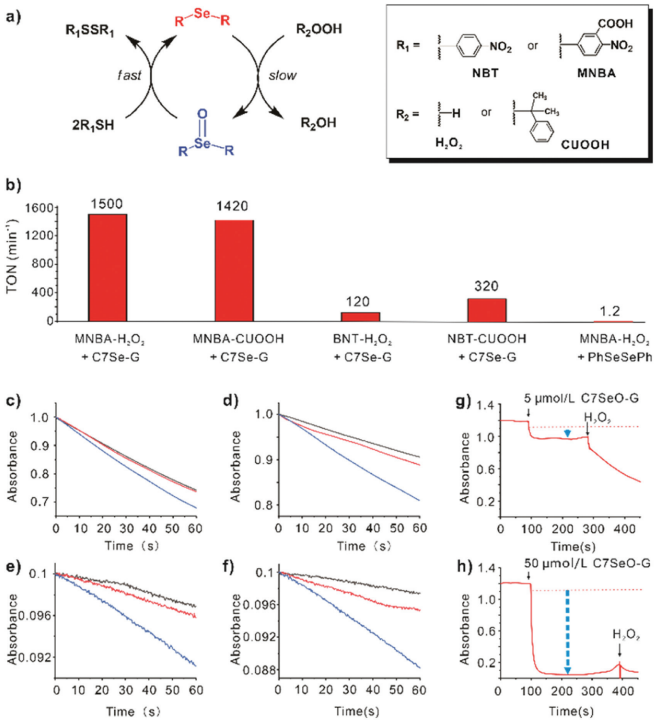

Fig. 4. (a) Redox cycle of selenides accelerates the formation of disulfides. Insert box: the structures of peroxides and water-soluble thiol substrates. (b) The turn over (TON) of the reaction. Plots of formation of disulfides from oxidation of monosulfides in (c) MNBA-H_2O_2, (d) MNBA-CUOOH, (e) NBT-H_2O_2, and (f) NBT-CUOOH assays with blank (black), 5 μmol/L (red), and 50 μmol/L (blue) C7Se-G in the DPBS buffer. Plots corresponding to the absorbance of $\lambda = 410$ nm before and after adding MNBA to the DPBS buffer containing different amount of C7SeO-G: (g) 5 μmol/L, (h) 50 μmol/L. The sudden jump of the curves indicated that the lid opening period of UV-vis spectrometer.

and the intermediate subsequently reacted efficiently with another thiol to form reduced C7Se-G and a disulfide product. As shown in Figs. 4g and h, the rapid consumption of MNBA upon the addition of C7SeO-G to the MNBA solution indicates that there was a reaction between C7SeO-G and MNBA. The reaction continued after the addition of H_2O_2 when MNBA was present in surplus in the system, confirming that selenoxides could be reconverted to selenides *via* the reduction of thiols, as shown in Fig. 4a. In addition, the NBT thiol cofactor reaction were similar to those of MNBA (Fig. S28 in Supporting information). Moreover, when a free-radical scavenger co-existed in the MNBA assay, the catalytic performance of C7Se-G did not disappear, indicating that the free-radical mechanism was not the dominat pathway in this reaction system (Fig. S29 in Supporting information). Unfortunately intermediate products such as selenium-containing hydroxy perhydroxy intermediates could not be determined by ESI-MS because of the abundant salt in the DPBS buffer [61].

In conclusion, a new class of guanidinium- and selenium-functionalized crown ether macrocyclic amphiphiles was developed. Mutating one atom and grafting a guanidinium group on crown ether provides an atom-economic approach for controlling hydration, responsiveness, dimension, and enhanced catalysis of macrocyclic amphiphiles. On the one hand, the selenium-containing crown ether itself provides an "All-In-One" building block. On the other hand, the amino-group equipment allows diverse functional groups can be grafted on, which made it easier to further integrate multiple functionalities through well-developed amine chemistry [5,17–21,24–26]. Therefore, we believe that the principle of current design also represents the principle of atom-economy for efficient usage of atoms to some extent. As illus-

tration, grafting guanidinium group readily affords the resulting macrocyclic amphiphile positively-charged solid nanoparticles formed in an aqueous medium, with redox-responsiveness in water. The resulting solid nanoparticles can capture the substrates more efficiently, consequently acting as potent nanozymes for catalyzing the reduction of peroxides and the formation of disulfide bonds. Thus far, there have been limited cases reporting the use of macrocyclic amphiphiles as nanozymes. Therefore, the fundamental results reported in this study not only present a new design form for organic selenide compounds but also pave the way for the construction of novel functional stimuli-responsive nanomaterials.

Declaration of competing interest

The authors declare that they have no known competing financial interests or personal relationships that could have appeared to influence the work reported in this paper.

Acknowledgments

We gratefully acknowledge financial support from the National Natural Science Foundation of China (Nos. 21901210, 22071196, 22007078), Key R&D Program of Shaanxi Province (No. 2021KWZ-18), Aeronautical Science Foundation of China (No. ASFC-2020Z061053001), Opening Project of State Key Laboratory of Polymer Materials Engineering (Sichuan University) (No. klpme2021-05-03), Student Innovation and Entrepreneurship Education Center of the Student Work Department of the Party Committee of NPU (No. 2021-cxcy-012), Fundamental Research Funds for the Central Universities, and Fellowship from CSC Innovative Team Program (No. CXXM20190099). We thank Dr. Boris Schade and Ms. Pinwei Lee for the measurements of cryo-TEM and SEM, respectively. We thank the Analytical & Testing Center of NPU for the characterization of materials

Supplementary materials

Supplementary material associated with this article can be found, in the online version, at doi:10.1016/j.cclet.2022.108015.

References

[1] D.E. Discher, R.D. Kamien, Nature 430 (2004) 519–520.
[2] C. Wang, Z. Wang, X. Zhang, Acc. Chem. Res. 45 (2012) 608–618.
[3] Li P, Chen Y, Y. Liu, Chin. Chem. Lett. 30 (2019) 1190–1197.
[4] K. Jie, Y. Zhou, Y. Yao, et al., Chem. Soc. Rev. 44 (2015) 3568–3587.
[5] G. Yu, K. Jie, F. Huang, Chem. Rev. 115 (2015) 7240–7303.
[6] Z. Xu, S.R. Jia, W. Wang, et al., Nat. Chem. 11 (2019) 86–93.
[7] X. Chi, G. Yu, L. Shao, et al., J. Am. Chem. Soc. 138 (2016) 3168–3174.
[8] L. Chen, J. Xiang, Y. Zhao, et al., J. Am. Chem. Soc. 140 (2018) 7079–7082.
[9] M. Hanafusa, Y. Tsuchida, K. Matsumoto, et al., Nat. Commun. 11 (2020) 6061.
[10] S. Himmelein, B.J. Ravoo, Chem. Eur. J. 23 (2017) 6034–6041.
[11] S. Sreejith, N.V. Menon, Y. Wang, et al., Mater. Chem. Front. 1 (2017) 831–837.
[12] G. Yu, Y. Ma, C. Han, et al., J. Am. Chem. Soc. 135 (2013) 10310–10313.
[13] X. Liu, K. Jia, Y. Wang, et al., ACS Appl. Mater. Interfaces 9 (2017) 4843–4850.
[14] K. Wang, J.H. Jordan, K. Velmurugan, et al., Angew. Chem. Int. Ed. 60 (2021) 9205–9214.
[15] K.M. Park, K. Baek, Y.H. Ko, et al., Angew. Chem. Int. Ed. 57 (2018) 3132–3136.
[16] B.M. Trost, Atom Economy: a Challenge for Enhanced Synthetic Efficiency, Handbook of Green Chemistry, Wiley-VCH Verlag GmbH & Co., 2010, pp. 1–35.
[17] G.W. Gokel, W.M. Leevy, M.E. Weber, Chem. Rev. 104 (2004) 2723–2750.
[18] Z. Zhang, Y. Yao, L. He, et al., Chin. Chem. Lett. 34 (2023) 107521.
[19] Y. Han, Z. Meng, Y.X. Ma, et al., Acc. Chem. Res. 47 (2014) 2026–2040.
[20] V.N. Vukotic, C.A. O'Keefe, K. Zhu, et al., J. Am. Chem. Soc. 137 (2015) 9643–9651.
[21] Z. Qi, C.A. Schalley, Acc. Chem. Res. 47 (2014) 2222–2233.
[22] J. Shang, H.L. Gong, Q. Zhang, et al., Chin. Chem. Lett. 32 (2021) 2005–2008.
[23] Q. Xu, Z. Cui, J. Yao, et al., Chin. Chem. Lett. 32 (2021) 4024–4028.
[24] H.G. Fu, Y. Chen, Y. Liu, ACS Appl. Mater. Interfaces 11 (2019) 16117–16122.
[25] Z.M. Tun, M.J. Panzner, V. Scionti, et al., J. Am. Chem. Soc. 132 (2010) 17059–17061.
[26] Z.H. Qi, P.M. de Molina, W. Jiang, et al., Chem. Sci. 3 (2012) 2073–2082.
[27] S. Dong, J. Leng, Y. Feng, et al., Sci. Adv. 3 (2017) eaao0900.
[28] Q. Zhang, T. Li, A. Duan, et al., J. Am. Chem. Soc. 141 (2019) 8058–8063.
[29] C. Perez, J.C. Lopez, S. Blanco, et al., J. Phys. Chem. Lett. 7 (2016) 4053–4058.
[30] S. Dong, L. Wang, J. Wu, et al., Langmuir 33 (2017) 13861–13866.
[31] X. Li, Y. Deng, J. Lai, et al., J. Am. Chem. Soc. 142 (2020) 5371–5379.
[32] X. Li, J.L. Lai, Y. Deng, et al., J. Am. Chem. Soc. 142 (2020) 21522–21529.
[33] Z. Qi, L. Chiappisi, H. Gong, et al., Chem. Eur. J. 24 (2018) 3854–3861.
[34] L. Jin, B. Li, Z.L.Y. Cui, et al., J. Phys. Chem. B 123 (2019) 9692–9698.
[35] E. Renault, J.Y. Le Questel, J. Phys. Chem. A 108 (2004) 7232–7240.
[36] W. Caminati, A. Dell'Erba, S. Melandri, et al., J. Am. Chem. Soc. 120 (1998) 5555–5558.
[37] Y.Y. Zhang, Y.Y. Liang, X.D. Zhao, ACS Catal. 11 (2021) 3755–3761.
[38] X.R. Xiao, C. Guan, J. Xiu, et al., Green Chem. 23 (2021) 4647–4655.
[39] H.G. Cao, R.R. Qian, L. Yu, Catal. Sci. Technol. 10 (2020) 3113–3121.
[40] C. Chen, Y.T. Cao, X.X. Wu, et al., Chin. Chem. Lett. 31 (2020) 1078–1082.
[41] J. Shang, S.R. Li, T.Z. Pan, et al., Chem. Commun. 56 (2020) 15052–15055.
[42] P. Farina, T. Latter, W. Levason, et al., Dalton Trans. 42 (2013) 4714–4724.
[43] P. Farina, W. Levason, G. Reid, et al., Polyhedron 55 (2013) 102–108.
[44] P.N. Bartlett, M.J.D. Champion, M.E. Light, et al., Dalton Trans. 44 (2015) 2953–2955.
[45] P. Farina, W. Levason, G. Reid, et al., Dalton Trans. 42 (2013) 89–99.
[46] W. Levason, S.D. Orchard, G. Reid, et al., Coord. Chem. Rev. 225 (2002) 159–199.
[47] R.G.S. Berlinck, D.I. Bernardi, T. Fill, et al., Natl. Prod. Rep. 38 (2021) 586–667.
[48] Q. He, G.I. Vargas-Zuniga, S.H. Kim, S.K. Kim, J.L. Sessler, Chem. Rev. 119 (2019) 9753–9835.
[49] T. Pan, J. Li, B. Li, et al., J. Phys. Chem. Lett. 12 (2021) 7418–7422.
[50] H.P. Xu, W. Cao, X. Zhang, Acc. Chem. Res. 46 (2013) 1647–1658.
[51] T.M. Hermans, M.A. Broeren, N. Gomopoulos, et al., Nat. Nanotechnol. 4 (2009) 721-726.
[52] R. Gleiter, D.B. Werz, B.J. Rausch, Chemistry 9 (2003) 2676–2683.
[53] D.B. Werz, R. Gleiter, F. Rominger, J. Am. Chem. Soc. 124 (2002) 10638–10639.
[54] G. Mugesh, W.W. du Mont, H. Sies, Chem. Rev. 101 (2001) 2125–2179.
[55] X. Xiao, Z. Shao, L. Yu, Chin. Chem. Lett. 32 (2021) 2933–2938.
[56] J. Shang, B. Li, X. Shen, et al., J. Org. Chem. 86 (2021) 1430–1436.
[57] Y. Huang, J. Ren, X. Qu, Chem. Rev. 119 (2019) 4357–4412.
[58] Y. Chong, J. Ning, S. Min, et al., Chin. Chem. Lett. 33 (2022) 3315–3324.
[59] J. Ma, J. Qiu, S. Wang, ACS Appl. Nano Mater. 3 (2020) 4925–4943.
[60] D. He, M. Yan, P. Sun, et al., Chin. Chem. Lett. 32 (2021) 2994–3006.
[61] V. Nascimento, E.E. Alberto, D.W. Tondo, et al., J. Am. Chem. Soc. 134 (2012) 138–141.
[62] Z.Y. Dong, J.Q. Liu, S.Z. Mao, et al., J. Am. Chem. Soc. 126 (2004) 16395–16404.